Available online at www.sciencedirect.com
ScienceDirect
Journal of Power Sources 167 (2007) 171–177
JOURNAL OF POWER SOURCES
www.elsevier.com/locate/jpowsour

$Ni_xCu_{6-x}Sn_5$ alloys as negative electrode materials for rechargeable lithium batteries

Jing-jun Zhang, Yi-min Zhang, Xiao Zhang, Yong-yao Xia *

Chemistry Department and Shanghai Key Laboratory of Molecular Catalysis and Innovative Materials, Fudan University, Shanghai 200433, China

Received 25 October 2006; received in revised form 2 February 2007; accepted 5 February 2007
Available online 17 February 2007

Abstract

A series of Ni doped $Ni_xCu_{6-x}Sn_5$ ($x = 0$, 0.5, 1, 2, 4) alloys were prepared by mechanical alloying, followed by annealing at 400 °C. The Ni doped alloys show the similar structure with that of Cu_6Sn_5 and Ni_3Sn_2, which can be indexed to a hexagonal Ni_2In type cell, but differ in the electrochemical performance as the anodes of Li-ion batteries. The electrochemical tests show that the cycling reversibility of $Ni_xCu_{6-x}Sn_5$ increases at the expense of the reversible capacity with the increasing amount of Ni content. The proper amount Ni doped alloy, $Ni_2Cu_4Sn_5$ showed better cycle performance with a reversible capacity of 200 mAh g^{-1} (1680 mAh ml^{-1}). The relative stability of the alloy was also investigated using the first-principles density-functional theory with pseudopotentials and plane wave basis (VASP).

Keywords: Alloys; Intermetallic compound; Tin; Lithium-ion batteries; First-principle calculation

1. Introduction

Metals and alloys present attractive alternatives to graphite as the anode materials for lithium-ion batteries due in particular to the high capacity, an acceptable rate capability, and operating potentials well above the potential of metallic lithium. In particular, the intermetallic compounds (M′M) show the most promising attentions [1–7]. It typically consists of an "inactive phase M′", which is referred to that does not react with lithium, and "active phase M", which is referred to that reacts with lithium. Introducing an "inactive phase, M′" can reduce the volume expansion/contraction in some extent, thus improving its cycling performance. According to the lithium-ion alloying mechanism, the alloys can be divided into two groups: the first one is referred to those alloys in which the reaction of lithium results first in the formation of $Li_xM'M$ as an intermediate phase, with further reaction leads to a mixed phase of the disordered Li_xM alloy and metal M′, and the initial intermetallic alloys are reformed when lithium was extracted from the alloys during charge, such as Cu_6Sn_5 [1,2], InSb [3,4], etc.; and the other one is referred to these alloys in which the reaction of lithium in the M′M results directly in the formation of a disordered Li_xM alloy and metal M′ matrix, but M′ cannot recombine with M to reform the initial intermetallic compounds during the charge, such as Sn–Mn [5], Sn–Fe [6], Co–Sn [7], etc. In the previous work, we studied the electrochemical performance of $Co_xCu_{6-x}Sn_5$ which has both the group I (Cu) and group II (Co) inactive metals. We have found that a proper amount of Co doped alloy, $CoCu_5Sn_5$, has the same structure with Cu_6Sn_5, and showed improved cycling stability at the expense of the capacity [7]. Compared with Co–Sn alloys, the Ni–Sn alloys, including Ni_3Sn_4, Ni_3Sn_2 and Ni_3Sn, in particular, the Ni_3Sn_2 and Ni_3Sn alloys which have the same Ni_2In-type structure with Cu_6Sn_5, are quite different in the electrochemical behavior from Co–Sn alloys: the pure crystalline Ni_3Sn_2 alloys prepared by mechanical alloying method have small reversible capacity (ca. 30 mAh g^{-1} [8], ca. 20 mAh g^{-1} [9]) but very good cycle performance; the pure crystalline electroplated Ni_3Sn_2 have a good cycle stability with a reversible capacity of 60–70 mAh g^{-1} [10]. Although the lithium alloying mechanism is not clear, it seems that the lithiation reaction results in the formation of Li_xNiSn, rather than the mixture phases of Li_xSn and Ni nanoparticles (lithium reaction with Co–Sn results in a mixture phase of $Li_{4.4}Sn$ and Co). In the present work, we used Ni to partly

* Corresponding author. Tel.: +86 21 55664177; fax: +86 21 55664177.
E-mail address: yyxia@fudan.edu.cn (Y.-y. Xia).

0378-7753/$ – see front matter © 2007 Elsevier B.V. All rights reserved.
doi:10.1016/j.jpowsour.2007.02.012

substitute Cu to prepare a series of Ni doped $Ni_xCu_{6-x}Sn_5$ ($x = 0$, 0.5, 1, 2, 4). The effects of doped-Ni amount on the structure and lithium intercalation were examined. The relationship between the electrochemical performance and the crystal structure was also studied by the first-principles calculation.

2. Experimental

2.1. Preparation and characterization

A series of Ni doped $Ni_xCu_{6-x}Sn_5$ ($x = 0$, 0.5, 1, 2, 4) alloys, i.e., Cu_6Sn_5, $Ni_{0.5}Cu_{5.5}Sn_5$, $NiCu_5Sn_5$, $Ni_2Cu_4Sn_5$ and $Ni_4Cu_2Sn_5$ were synthesized by mechanical ball-milling stoichiometric amount of metallic powder Cu, Ni and Sn for 12 h under Ar atmosphere using a high-energy planetary mono mill pulverisette 6 (Fritsch GmbH Inc., Germany). After milling, the powders were pressed into pellets and heat-treated at 400 °C for 12 h under Ar flow in order to obtain single phase, well crystalline intermetallic compounds. The gray brittle products were then ground and sifted to approximately 400 mesh. The Ni–Sn alloys (Ni_3Sn, Ni_3Sn_2 and Ni_3Sn_4) were also prepared by the same process mentioned above from Ni and Sn metallic powders.

X-ray diffraction (XRD) patterns of the powdered samples were obtained using an X-ray diffractometer (Bruker Advance8) with Cu Kα radiation. The diffraction data were collected at 0.015 step widths over a 2θ range from 20 to 85°. The structural parameters were refined by Rietveld analysis using the computer program RIETAN 2000. The structural model used is the Ni_2In-type structure (space group $P6_3/mmc$, no. 194).

The electrodes were prepared by mixing 80% alloy powders, 10% carbon black and 10% polyvinylidene fluoride (PVDF) dissolved in *N*-methylpyrrolidinone (NMP). The slurries of the mixture were coated on Cu foil. After coating, the electrodes were dried at 80 °C for 10 min to remove the solvent before pressing. The electrodes were cut into sheets 1 cm^2 in area, vacuum-dried at 100 °C for 24 h, and weighed. The typical weight load of active material is about 5 mg cm^{-2}. The battery performance of alloy was characterized in CR2032-type coin cell. Metallic lithium was used as the negative electrode. The electrolyte solution was 1 M $LiPF_6$/ethlylene carbonate (EC)/dimethyl carbonate (DMC)/ethyl methyl carbonate (EMC) (1:1:1 by volume). The cells were cycled at a constant current density of 0.25 mA cm^{-2} between 0.0 and 2.0 V. Lithium insertion into an alloy electrode was referred to as discharge and extraction as charge. The cell capacity was determined by only the alloy active material.

2.2. Computational

To investigate the relative stability of the $Ni_xCu_{6-x}Sn_5$ alloys, we defined the formation energy of $Ni_xCu_{6-x}Sn_5$ alloys as the following functions:

$$E_f = E_{Ni_xCu_{6-x}Sn_5} - \frac{6-x}{6}E_{Cu_6Sn_5} - \frac{x}{3}E_{Ni_3Sn_2} - \frac{x}{6}E_{Sn} \quad (1)$$

where E_f is the formation energy of $Ni_xCu_{6-x}Sn_5$ alloys and E_C is the total energy of compound C. The total energy of alloys $Ni_xCu_{6-x}Sn_5$ ($x = 0$, 1, 2, 3, 4, 5, 6), Ni_3Sn_2 and metal Sn are calculated using the first-principles calculation based on the density-functional theory with pseudopotentials and plane wave basis (VASP) [11,12].

In order to investigate the difference of lithiation in alloys of Cu_6Sn_5 and Ni_3Sn_2, we performed the relative energy calculations for the lithiated alloys of $Li_xCu_6Sn_5$ and $Li_xNi_3Sn_2$ in which the Li occupied in the high symmetric vacant sites, and the alloys of Li_xSn appeared in the lithiation process after the inert metal extracted from the alloy matrix. The relative energy for the compound Li_xM_ySn is given as:

$$E_r = E_{Li_xM_ySn} + (4.4 - x)E_{Li} - E_{Li_{4.4}Sn} - yE_M \quad (2)$$

where E_r is the relative energy of Li_xM_ySn alloys and E_C is the total energy of compound C.

The Cu_6Sn_5 compound and the Ni doped alloys used in the computational study were chosen as a defect Ni_2In type structure in which Sn occupying 2c (1/3, 2/3, 1/4) position and Cu (Ni) at the 2a (0, 0, 0) and 2d (1/3, 2/3, 3/4) positions of space group $P6_3/mmc$. The Cu (Ni) occupancy of the 2a position is 100% and 2d position was 20% for $Ni_xCu_{6-x}Sn_5$ ($x = 0$, 1, 2, 3, 4, 5), every fifth trigonal bipyramidal site in the strings of Sn atoms [13]. For Ni_3Sn_2, the Ni occupancy of 2a is 100% and 2d is 50% [14]. The structure of metal Sn used in the calculation is tetragonal $I4_1/amd$ (no. 141) [15].

The number of atoms per unit cells was 22 for $Ni_xCu_{6-x}Sn_5$ ($x = 0$, 1, 2, 3, 4, 5) and 4 for metal Sn, depending on which the desired sets of *k*-points in reciprocal space were chosen. In all of the calculations, the convergence of the total energy with respect to *k*-point sampling and plane wave energy cutoff has been carefully examined. The final set of energies was computed with an energy cutoff of 500 eV for all compounds. The *k* point number of 62 and 196 for $Co_xCu_{6-x}Sn_5$ ($x = 0$, 1, 2, 3, 4, 5, 6) and metal Sn has been used, respectively, for the irreducible Brillouin zone integration.

3. Results and discussion

3.1. Structure and cycle performance of Ni–Sn alloys

Fig. 1 shows the X-ray diffraction patterns of Ni_3Sn, Ni_3Sn_2 and Ni_3Sn_4. No Ni, Sn, or oxides diffraction peaks are observed, which are well agreement with the previous reports [8,9,16]. The Ni_3Sn and Ni_3Sn_2 can be indexed to the hexagonal $P6_3/mmc$ structure, and the Ni_3Sn_4 to the monoclinic $C2/m$ structure. The capacity *versus* cycle number plots for the alloys are shown in Fig. 2. Small reversible capacity is observed for all the three alloys, while the cycle performance is very good, especially for the Ni_3Sn_2.

3.2. Characterization of $Ni_xCu_{6-x}Sn_5$

As mentioned in Section 1, the Ni_3Sn_2 and Ni_3Sn alloys have the same Ni_2Sn-type structure with Cu_6Sn_5 which has relative high capacity of ca. 500 mAh g^{-1}. We are interested in studying the electrochemical performance of Ni doped $Ni_xCu_{6-x}Sn_5$.

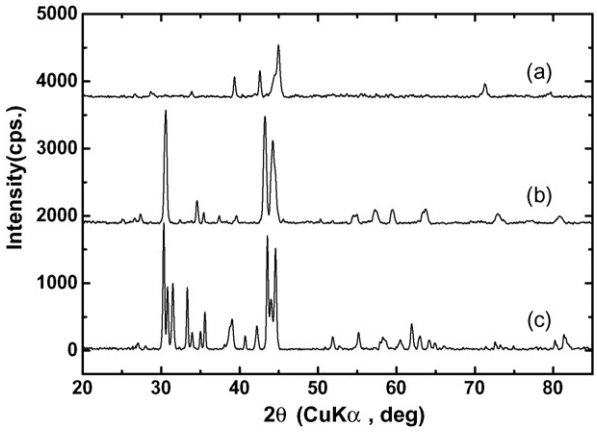

Fig. 1. Powder XRD patterns of Ni–Sn alloys: (a) Ni_3Sn, (b) Ni_3Sn_2 and (c) Ni_3Sn_4.

Fig. 3 compares the X-ray diffraction patterns of $Ni_xCu_{6-x}Sn_5$ powders with that of Cu_6Sn_5 and Ni_3Sn_2. As shown in Fig. 3, all patterns are very similar and can be ascribed to the signature peaks corresponding to the hexagonal structure $P6_3/mmc$. No peaks corresponding to Cu or Ni are detected. However, as a result of substituting Cu with Ni, the diffraction patterns are varied slightly. Firstly, it is obvious that the (0 0 2) and (0 0 4) peaks slightly shift to the small angle, while the other peaks shift to the large angle with increasing amount of doped-Ni content. Secondly, the two diffraction peaks, (1 1 0) and (1 0 2), around 42° overlap first and then split again with increasing amount of doped-Ni content. The peak of (1 1 0) shifts gradually from the left to (1 0 2) peak on Cu_6Sn_5 pattern to the right to the (1 0 2) peak on the pattern of Ni_3Sn_2. It can be deduced that the shift amount of (1 1 0) peak is large than that of (1 0 2) peak. The lower intensity and broad peaks of Ni_3Sn_2 indicate smaller particle size of Ni_3Sn_2.

In order to investigate the change of lattice parameters, we performed the Rietveld refinement. For the refinement, we use the same structure as the first-principles calculation described in the computational section. The refined lattice parameters are listed in Table 1. All patterns were fitted successfully to the model structure. The refinement results show that the lattice parameter a, and the cell volume decrease, while the lattice parameter c increases with the increasing Ni content in $Ni_xCu_{6-x}Sn_5$.

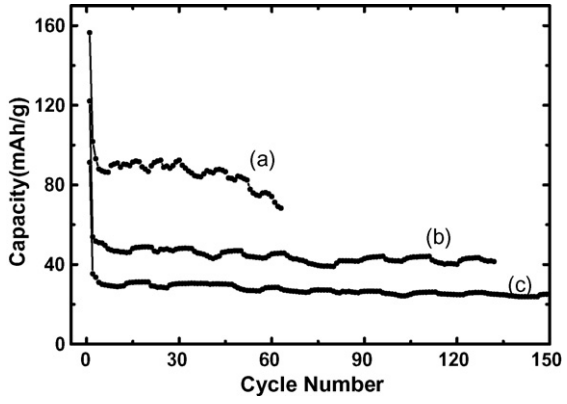

Fig. 2. Capacity *vs.* cycle number of Li/Ni–Sn alloy cells containing: (a) Ni_3Sn_4, (b) Ni_3Sn and (c) Ni_3Sn_2 at a current of 0.25 mA cm^{-2} between 0 and 1.2 V.

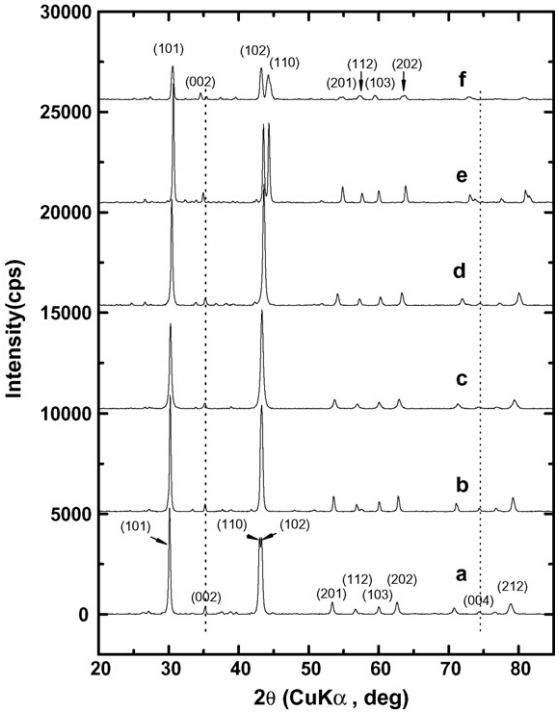

Fig. 3. Powder XRD patterns of $Ni_xCu_{6-x}Sn_5$ alloys: (a) Cu_6Sn_5, (b) $Ni_{0.5}Cu_{5.5}Sn_5$, (c) $NiCu_5Sn_5$, (d) $Ni_2Cu_4Sn_5$, (e) $Ni_4Cu_2Sn_5$ and (f) Ni_3Sn_2. The miller index for each peak of Cu_6Sn_5 and Ni_3Sn_2 is marked in the figure.

Since the similarity of the crystal structure of Cu_6Sn_5 and Ni_3Sn_2, it is important to see whether the Ni doped $Ni_xCu_{6-x}Sn_5$ alloys consist of a single phases or multiphase coexistence of Cu_6Sn_5 and Ni_3Sn_2. We applied the first-principles calculation to study their thermodynamic stability based on the density-functional theory with pseudopotentials and plane wave basis (VASP). The volume per formula unit and the formation energy of $Ni_xCu_{6-x}Sn_5$ as defined in Section 2.2 are shown in Fig. 4(A and B). We can see that the cell volume per formula unit is decreases with increasing amounts of Ni in $Ni_xCu_{6-x}Sn_5$ as shown in Fig. 4(A). This is well agreement with the results of XRD and the Rietveld refinement. The formation energy of $Ni_xCu_{6-x}Sn_5$ is negative with respect to the sum of

Table 1
Rietveld refinement results for $Ni_xCu_{6-x}Sn_5$

Samples	Phase	Rietveld refinement results				
		a (=b) (Å)	c (Å)	V (Å^3)	R_{wp} (%)	R_p (%)
Cu_6Sn_5	$P6_3/mmc$	4.196	5.088	77.58	7.12	5.46
$Ni_{0.5}Cu_{5.5}Sn_5$	$P6_3/mmc$	4.191	5.098	77.55	6.25	4.79
$NiCu_5Sn_5$	$P6_3/mmc$	4.181	5.104	77.27	4.92	3.77
$Ni_2Cu_4Sn_5$	$P6_3/mmc$	4.147	5.118	76.23	5.46	4.12
$Ni_4Cu_2Sn_5$	$P6_3/mmc$	4.086	5.134	74.23	5.79	4.29
Ni_3Sn_2	$P6_3/mmc$	4.090	5.186	75.13	6.23	4.72

a, c and V are the two lattice constants and cell volume of the structures, respectively. R_{wp} and R_p are the two quantities describing the goodness of fit and the agreement between the calculated and observed intensities, respectively.

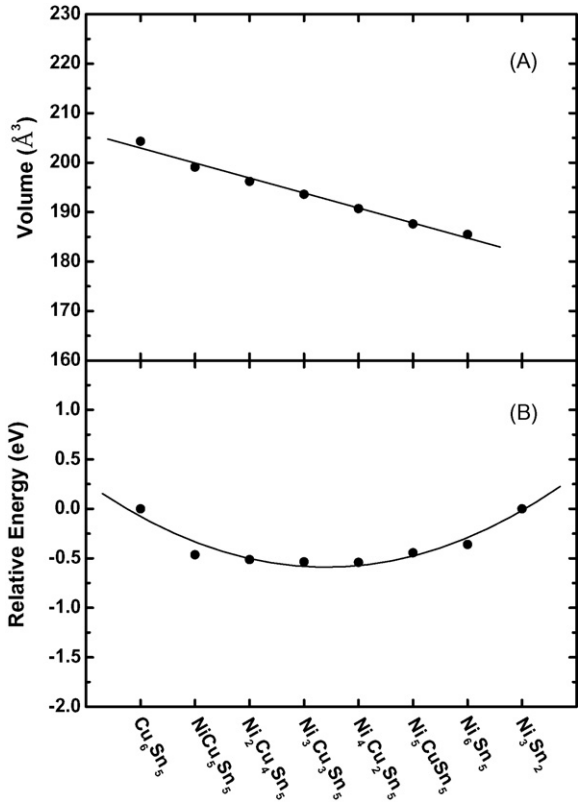

Fig. 4. The cell volume per formula unit (A) and the calculated relative energy (B) for $Ni_xCu_{6-x}Sn_5$ ($x = 0$, 0.5, 1, 2, 4) and Ni_3Sn_2.

energies for $(6-x)/6Cu_6Sn_5$, $x/3Ni_3Sn_2$ and $x/6Sn$, suggesting that it is possible thermodynamically that the $Ni_xCu_{6-x}Sn_5$ form homogeneous solid matrix in a unit cell level rather than simple mixture of Cu_6Sn_5, Ni_3Sn_2 and Sn crystals.

3.3. Electrochemical performance

Fig. 5 shows the typical charge/discharge profiles of Cu_6Sn_5, $Ni_xCu_{6-x}Sn_5$ and Ni_3Sn_2 alloy electrodes at a current rate of 0.25 mA cm^{-2} between 0.0 and 1.2 V. It is clear from Fig. 5(A) that Cu_6Sn_5 reveals two plateaus on discharge (lithiation), one at about 0.4 V and the other below 0.15 V *versus* Li/Li$^+$, corresponding to the transformation from hexagonal Cu_6Sn_5 to the intermediate phase of cubic $Li_xCu_6Sn_5$ and $Li_{4.4-x}Sn + Cu$ phases. Accordingly, two regions are observed on the charge (delithiation), one below 0.5 V and the other between 0.5 and 0.8 V *versus* Li/Li$^+$. The result is well agreement with the previous reports [1,2]. For the small Ni substituted alloys $Ni_{0.5}Cu_{5.5}$ and $NiCu_5Sn_5$, as shown in Fig. 5(B and C), the initial discharge curves are different form that of Cu_6Sn_5. Slightly smaller first discharge capacity is observed and the plateau of 0.4 V is disappeared gradually on the first discharge curve. Moreover, the capacity released up 0.15 V increase and the capacity below 0.15 V decrease with the increasing amount of Ni substituted. The subsequent charge/discharge curve shows that the plateaus of 0.4 V on discharge and 0.8 V on charge became smaller and finally undistinguishable, the reversible capacity decreases gradually and the cycling ability improves with the increasing

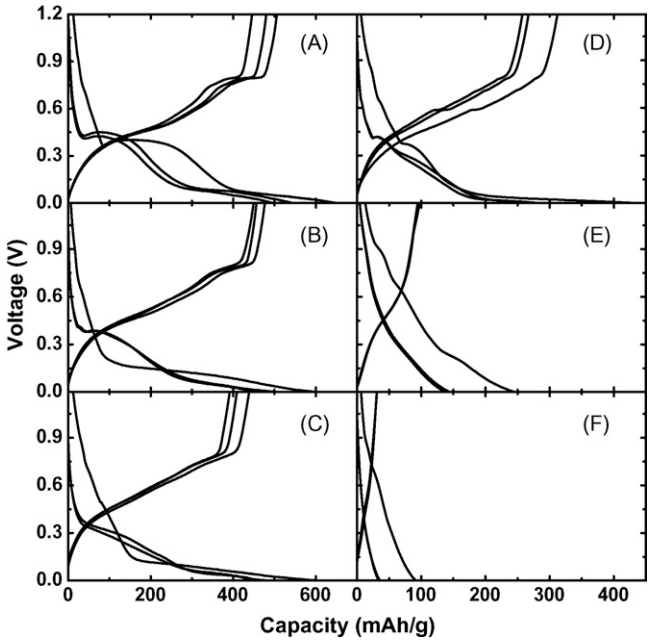

Fig. 5. Typical first three charge/discharge curves of Li/alloy cells containing Cu_6Sn_5 (A), $Ni_{0.5}Cu_{5.5}Sn_5$ (B), $NiCu_5Sn_5$ (C), $Ni_2Cu_4Sn_5$ (D), $Ni_4Cu_2Sn_5$ (E) and Ni_3Sn_2 (F).

amount of Ni substituted (see Fig. 3). For the larger Ni content alloys of $Ni_2Cu_4Sn_5$, the charge/discharge curve changes very much, the capacity is much less than that of Cu_6Sn_5 and the curve shows multiple potential plateaus which is very similar with that of the Sn electrode reported by Yang et al. [17]. This profile indicates that the Li alloying mechanism is very much different with that of small Ni doped alloys, the structure of $Ni_2Cu_4Sn_5$ may not be stable and probably some Sn extract form the alloy during Li alloying reaction. Finally, for the alloys of $Ni_4Cu_2Sn_5$ and Ni_3Sn_2, the capacity dramatically decreases and the charge/discharge profile became slippery. Table 2 summarizes the first charge/discharge capacity and coulomb efficiency of $Ni_xCu_{6-x}Sn_5$ alloy electrodes. The capacity and coulomb efficiency decrease with the increasing amount of Ni content in the alloys.

Fig. 6 compares the charge–discharge cycling of Li/alloy cells containing $Ni_xCu_{6-x}Sn_5$ ($x = 0$, 0.5, 1, 2, 4) and Ni_3Sn_2 alloys at a current rate of 0.25 mA cm^{-2} between 0 and 1.2 V. As shown in Fig. 4 that the cycling ability gradually improves as the Ni content increases in the alloys. The Cu_6Sn_5 has high capacity but poor cycling ability and the Ni_3Sn_2 has very good cycling ability but very low capacity. The low Ni doped alloys of $Ni_{0.5}Cu_{5.5}Sn_5$ and $NiCu_5Sn_5$ have high capacity and better cycling performance than Cu_6Sn_5. And the $Ni_2Cu_4Sn_5$ and $Ni_4Cu_2Sn_5$ have good cycling ability with a reversible capacity of ca. 200 mAh g^{-1} (1680 mAh ml^{-1}).

3.4. The phase transformation study by first-principles calculation

In order to investigate why Cu_6Sn_5 and Ni_3Sn_2 alloys have the similar structure, but differ in the electrochemical

Table 2
Summaries in the first charge/discharge capacity and efficiency of the alloys

Alloys	Density ($g\,ml^{-1}$)	First discharge capacity		First charge capacity		Coulomb efficiency (%)
		($mAh\,g^{-1}$)	($mAh\,ml^{-1}$)	($mAh\,g^{-1}$)	($mAh\,ml^{-1}$)	
Cu_6Sn_5	8.35	651	5436	515	4300	79.1
$Ni_{0.5}Cu_{5.5}Sn_5$	8.33	599	4990	457	3807	76.3
$Ni_1Cu_5Sn_5$	8.34	600	5004	440	3670	73.3
$Ni_2Cu_4Sn_5$	8.41	436	3667	312	2624	71.6
$Ni_4Cu_2Sn_5$	8.55	246	2103	100	855	40.7
Ni_3Sn_2	9.14	91	832	31	283	34.1

performance: Cu_6Sn_5 has large capacity but poor cycling stability, while Ni_3Sn_2 has small capacity but good cycle stability, we carried out the relative energy calculations using the first-principles density-functional theory with pseudopotentials and plane wave basis (VASP). For the Cu_6Sn_5, the phase transformation from Cu_6Sn_5 to the Li_2CuSn-type structure occurs by a topotactic transformation in which 50% of the Sn atoms in the framework are cooperatively displaced into neighboring trigonal bipyramidal sites, thereby dislodging the interstitial Cu atoms form these sites and extruding them form the structure [18,19]. The study of Sharma et al. proposed that after the insertion of two Li atoms per Cu_6Sn_5 formula unit, 1/6 of the Cu atoms are extruded from the structure, leading to a large structure rearrangement, to form Li_2CuSn [20]. Moreover, Larcher et al. reported that the phase Li_2CuSn can have a variable stoichiometry ($Li_{2-x}CuSn$) during the charge (delithiation) process above 0.5 V [2]. In the structure of Cu_6Sn_5 cells, as mentioned in Section 2.2, 20% 2d sites are occupied by Cu atoms, leaving other 80% 2d sites vacant. Based on the previous studies and the character of the Cu_6Sn_5 cells, we first introduce a few Li atoms in the interstitial voids of 2d sites keeping the original hexagonal structure ($P6_3/mmc$), and calculate the relative energies of $Li_xCu_6Sn_5$ ($x = 0.0, 0.5, 1.0, 2.0, 3.0$) to see the reaction of lithiation is energetic preferable or hindered. During the further lithiation from $Li_2Cu_6Sn_5$ to the cubic Li_2CuSn, we performed the calculation of the intermediate phase of $Li_{2-x}CuSn$ ($x = 1.25, 1.0, 0.5, 0.0$, from the hexagonal to cubic structure). Then, we supposed that the Cu atoms replaced by the Li atoms and extrude form the structure of Li_2CuSn, leaving a compound of Li_3Sn. The further lithiation lead to the formation of Li–Sn intermetallic compounds of Li_7Sn_2 [21] and $Li_{4.4}Sn$ [22]. The structure details used in the calculation are listed in Table 3. In the total energy calculation, when more than one arrangement exists for one compound, the lowest energy arrangement is chosen. As shown in Fig. 7, the relative energy of the compounds become lower gradually during lithium alloying process of Cu_6Sn_5, indicating the lithiated compound is energetically stable and the lithiation process is energetically preferable. Moreover, when the Li content introduced to the interstitial void of Cu_6Sn_5 matrix reaches to about 2, which means that a little more than 50% interstitial void of 2d sites have been occupied, the structural transformation energy form the hexagonal structure to the cubic Li_2CuSn-tpye structure become small enough to make it happen. Also, the calculated relative energies and the experimental first charge/discharge curve are compared in Fig. 7. We can see some similarity

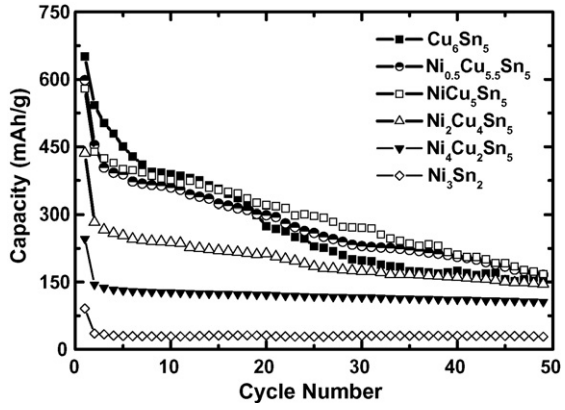

Fig. 6. Capacity *vs.* cycle number of Li/alloy cells containing $Ni_xCu_{6-x}Sn_5$ ($x = 0, 0.5, 1, 2, 4$) and Ni_3Sn_2 at a current of $0.25\,mA\,cm^{-2}$ between 0 and 2.0 V.

Table 3
Crystal structure information used in the calculation

Name	Space group	Structure	Reference
Cu_6Sn_5	$P6_3/mmc$	$(Cu_5)^{2a}(Cu)^{2d}(Sn_5)^{2c}$	[13]
$Li_{0.5}Cu_6Sn_5$	$P6_3/mmc$	$(Cu_5)^{2a}(Li_{0.5}Cu)^{2d}(Sn_5)^{2c}$	
$LiCu_6Sn_5$	$P6_3/mmc$	$(Cu_5)^{2a}(LiCu)^{2d}(Sn_5)^{2c}$	
$Li_2Cu_6Sn_5$	$P6_3/mmc$	$(Cu_5)^{2a}(Li_2Cu)^{2d}(Sn_5)^{2c}$	
$Li_3Cu_6Sn_5$	$P6_3/mmc$	$(Cu_5)^{2a}(Li_3Cu)^{2d}(Sn_5)^{2c}$	
$Li_{0.75}CuSn$	F-43m	$Sn^{4a}(Li_{0.75})^{4b}Cu^{8c}$	
$LiCuSn$	F-43m	$Sn^{4a}Li^{4b}Cu^{8c}$	
$Li_{1.5}CuSn$	F-43m	$Sn^{4a}Li^{4b}(Li_{0.5})^{8c}Cu^{8c}$	
Li_2CuSn	F-43m	$Sn^{4a}Li^{4b}Li^{8c}Cu^{8c}$	[24]
Li_3Sn	F-43m	$Sn^{4a}Li^{4b}(Li_2)^{8c}$	
$Li_{3.5}Sn(Li_7Sn_2)$	$Cmmm$	See ref. [21]	[21]
$Li_{4.4}Sn$	$F23$	See ref. [22]	[22]
Ni_3Sn_2	$P6_3/mmc$	$(Ni_2)^{2a}(Sn_2)^{2c}Ni^{2d}$	[14]
$Li_{0.5}Ni_3Sn_2$	$P6_3/mmc$	$(Ni_2)^{2a}(Sn_2)^{2c}Ni^{2d}(Li_{0.5})^{2d}$	
$LiNi_3Sn_2$	$P6_3/mmc$	$(Ni_2)^{2a}(Sn_2)^{2c}Ni^{2d}Li^{2d}$	
$Li_2Ni_3Sn_2$	$P6_3/mmc$	$(Ni_2)^{2a}Li^{2b}(Sn_2)^{2c}Ni^{2d}Li^{2d}$	
$Li_{0.25}NiSn$	F-43m	$Ni^{4a}Li_{0.25}{}^{4b}Cu^{8c}$	
$Li_{0.5}NiSn$	F-43m	$Ni^{4a}Li_{0.5}{}^{4b}Cu^{8c}$	
$LiNiSn$	F-43m	$Ni^{4a}Li^{4b}Cu^{8c}$	
Li_2NiSn	F-43m	$Ni4a_{Li}4b_{Li}8c_{cu}8c$	
Li_3Sn	F-43m	$Sn^{4a}Li^{4b}(Li_2)^{8c}$	
$Li_{3.5}Sn(Li_7Sn_2)$	$Cmmm$	See ref. [21]	[21]
$Li_{4.4}Sn$	$F23$	See ref. [22]	[22]

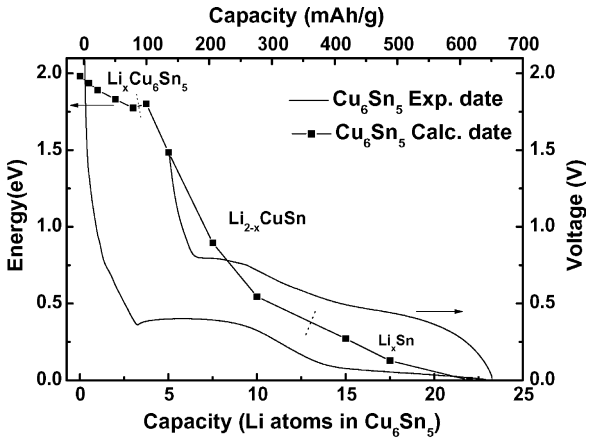

Fig. 7. Comparison between the calculated reaction path (in relative energy formation) and the experimental electrochemical voltage profile for Cu_6Sn_5.

between the calculated reaction path (in the energy format) and the experiment reaction path (in the voltage format).

Up to date, very few works have been reported about the crystal structure of the lithiated Ni–Sn alloys. Therefore, we calculated the relative energies for the Ni_3Sn_2 and its lithiated alloys in the same way as Cu_6Sn_5 as shown in Fig. 8. The crystal structure information used in the calculations is shown in Table 3. For the Ni_3Sn_2 cells, there are only 50% interstitial 2d sites vacant (in this Li content level for Cu_6Sn_5 cells, the structure become unstable and the transformation to the cubic cells begins to happen). When we introduced the Li atoms to the interstitial voids of 2d sites in which it keeps the original hexagonal structure, the relative energies of $Li_xNi_3Sn_2$ ($x = 0.5$, 1.0) were almost the same with that of Ni_3Sn_2 as shown in Fig. 8. It indicates that the Li alloying in the Ni_3Sn_2 is very difficult. Further introducing the Li atoms to the interstitial voids of 2b sites causes the relative energy increases dramatically, which means that the intercalated Li content level of Li:Sn > 1:2 is energetically hindered for Ni_3Sn_2. The electrochemical tests show that the reversible capacity of Ni_3Sn_2 is ca. 30 mAh g^{-1} even in the small charge/discharge current of 0.05 mA cm^{-2} (ca. 10 μA mg^{-1}). Moreover, we further ball-milled the as prepared Ni_3Sn_2 alloy for 20 h at the speed of 400 r/s at the Ar gas atmosphere in order to crush the particle size, and then tested its capacity. We got a reversible capacity of 60–70 mAh g^{-1} (about 1 atom per Ni_3Sn_2). However, the increased capacity is very likely from the reaction of Li with the increased grain-boundary Sn atoms [23]. The detail reaction mechanism of Li with Ni_3Sn_2 is to be further investigated.

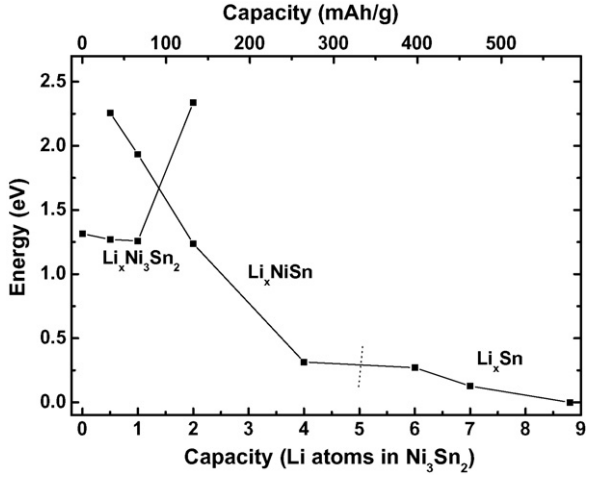

Fig. 8. The relative energy calculations of the Ni_3Sn_2 alloys and their lithiated products.

Moreover, in order to investigate the possibility of phase transformation from the hexagonal cells to the cubic cells like Cu_6Sn_5, we also calculated the relative energies of the cubic Li_xNiSn ($x = 0.25$, 0.5, 1.0, 2.0) structure (like Li_xCuSn, the model structures supposed that the same structure transformation with Cu_6Sn_5 occurs in Ni_3Sn_2) as shown in Fig. 8. The relative energies of the cubic Li_xNiSn are higher than that of the hexagonal $Li_xNi_3Sn_2$ at the same/close Li content level when Li:Sn < 1/2. Although, the relative energies of the further lithiated Li_xSn (over $LiNi_3Sn_2$) are smaller than that of $LiNi_3Sn_2$ as shown in Fig. 8, the reaction cannot occur through the phase transformation from the hexagonal to cubic structure as the way of Cu_6Sn_5 because of the high-energy barrier. Base on the above calculation, we speculated that the structure rearrangement from the hexagonal cells to the cubic cells is energetically hindered for the Ni_3Sn_2 during the reaction with Li, and this might be the reason that results in the small capacity of Ni_3Sn_2 comparing with Cu_6Sn_5.

4. Conclusion

Ni doped $Ni_xCu_{6-x}Sn_5$ ($x = 0$, 0.5, 1, 2, 4) alloys show the similar structure, but different electrochemical performance, with that of Cu_6Sn_5 and Ni_3Sn_2. The first-principles calculation calculations suggest that the Ni doped alloys are the single phase intermetallic compounds instead of the mixture phase of Cu_6Sn_5, Ni_3Sn_2 and metal Sn. The electrochemical tests show that the cycle performance improves while the reversible capacity decreases with the increasing amount of Ni content. A proper amount of Ni doped alloy, $NiCu_5Sn_5$ and $Ni_2Cu_4Sn_5$ show an improved cycling stability with a reversible capacity of 200 mAh g^{-1} (1680 mAh ml^{-1}). The first-principles calculations suggest that the lithiation depth of Cu_6Sn_5 can reach to $Li_{4.4}Sn$, however, the reversible capacity is very small for Ni_3Sn_2 and it may attribute to the high-energy barrier required for the structure transformation from the hexagonal structure to the cubic structure.

Acknowledgments

Financial supports from National Natural Science Foundation of China (No. 20373014), and the Project Sponsored by the Scientific R0esearch Foundation for the Returned Overseas Chinese Scholars, State Education Ministry is acknowledged. The calculation is supported by Fudan High-end Computing Center.

References

[1] K.D. Kepler, J.T. Vaughey, M.M. Thackeray, Electrochem. Solid-State Lett. 2 (1999) 307.
[2] D. Larcher, L.Y. Beaulieu, D.D. MacNeil, J.R. Dahn, J. Electrochem. Soc. 147 (2000) 1658.
[3] J.T. Vaughey, J. O'Hara, M.M. Thackeray, Electrochem. Solid-State Lett. 3 (2000) 13.
[4] K.C. Hewitt, L.Y. Beaulieu, J.R. Dahn, J. Electrochem. Soc. 148 (2001) A402.
[5] L.Y. Beaulieu, J.R. Dahn, J. Electrochem. Soc. 147 (2000) 3237.
[6] O. Mao, R.A. Dunlap, J.R. Dahn, J. Electrochem. Soc. 146 (1999) 405.
[7] J.J. Zhang, Y.Y. Xia, J. Electrochem. Soc. 153 (2006) A1466.
[8] Y.L. Kim, H.Y. Lee, S.W. Jang, S.J. Lee, H.K. Baik, Y.S. Yoon, Y.S. Park, S.M. Lee, Solid State Ionics 160 (2003) 235.
[9] G.M. Ehrlich, C. Durand, X. Chen, T.A. Hugener, F. Spiess, S.L. Suib, J. Electrochem. Soc. 147 (2000) 886.
[10] O. Crosnier, T. Brousse, X. Devaux, P. Fragnaud, D.M. Schleich, J. Power Sources 94 (2001) 169.
[11] G. Kresse, J. Furthmuller, Comput. Mater. Sci. 6 (1996) 15.
[12] G. Kresse, J. Furthmuller, Phys. Rev. B 54 (1996) 11169.
[13] A.K. Larsson, L. Stenberg, S. Lidin, Acta Crystallogr. Sect. B-Struct. Sci. 50 (1994) 636.
[14] M. Ellner, J. Less-Common Met. 48 (1976) 21.
[15] M. Liu, L.-G. Liu, High Temp. High Pressures 18 (1986) 79.
[16] H.Y. Lee, S.W. Jang, S.M. Lee, S.J. Lee, H.K. Baik, J. Power Sources 112 (2002) 8.
[17] J. Yang, Y. Takeda, N. Imanishi, O. Yamamoto, J. Electrochem. Soc. 146 (1999) 4009.
[18] M.M. Thackeray, J.T. Vaughey, A.J. Kahaian, K.D. Kepler, R. Benedek, Electrochem. Commun. 1 (1999) 111.
[19] G.X. Wang, L. Sun, D.H. Bradhurst, S. Zhong, S.X. Dou, H.K. Liu, J. Power Sources 88 (2000) 278.
[20] S. Sharma, L. Frasson, E. Sjöstedt, L. Nordström, B. Johansson, K. Edström, J. Electrochem. Soc. 150 (2003) A330.
[21] I.A. Courtney, J.S. Tse, O. Mao, J. Hafner, J.R. Dahn, Phys. Rev. B 58 (1998) 15583.
[22] J.R. Dahn, I.A. Courtney, O. Mao, Solid State Ionics 111 (1998) 289.
[23] L.Y. Beaulieu, D. Larcher, R.A. Dunlap, J.R. Dahn, J. Electrochem. Soc. 147 (2000) 3206.
[24] H.-U. Schuster, Naturwissenschaften 53 (1966) 360.